

Generation and Characterization of Large Non-Gaussianities in Single Field Inflation

Xingang Chen¹, Richard Easther² and Eugene A. Lim³

¹ Center for Theoretical Physics,
Massachusetts Institute of Technology, Cambridge, MA 02139

² Department of Physics, Yale University, New Haven, CT 06511

³ ISCAP and Physics Department, Columbia University, New York, NY 10027

Abstract

Inflation driven by a single, minimally coupled, slowly rolling field generically yields a negligible primordial non-Gaussianity. We discuss two distinct mechanisms by which a non-trivial potential can generate large non-Gaussianities. Firstly, if the inflaton traverses a feature in the potential, or if the inflationary phase is short enough so that initial transient contributions to the background dynamics have not been erased, modes near horizon-crossing can acquire significant non-Gaussianities. Secondly, potentials with small-scale structure may induce significant non-Gaussianities while the relevant modes are deep inside the horizon. The first case includes the “step” potential we previously analyzed while the second “resonance” case is novel. We derive analytic approximations for the 3-point terms generated by both mechanisms written as products of functions of the three individual momenta, permitting the use of efficient analysis algorithms. Finally, we present a significantly improved approach to regularizing and numerically evaluating the integrals that contribute to the 3-point function.

Contents

1	Introduction	1
2	Single scalar field inflation models and Maldacena’s formalism	3
3	Numerical integration	4
4	Horizon scale generation of non-Gaussianities	7
4.1	Features in the inflationary potential	7
4.2	Non-attractor initial conditions	11
5	Sub-horizon generation of non-Gaussianities: Resonance model	13
6	Discussion and Conclusion	17
A	3-point correlation functions	19
B	Non-Gaussianities from initial conditions	21
C	Slow-roll parameters in the resonance model	23

1 Introduction

The primordial power spectrum or 2-point correlation function of the temperature anisotropies in the Cosmic Microwave Background (CMB) is well-measured out to large multipoles. The higher moments of a distribution are, in general, independent of the 2-point function, but the CMB anisotropies are at least approximately Gaussian. Theoretically, we know that non-Gaussian component to the CMB will always be induced by non-linear gravitational couplings between modes after they reenter the horizon [1] while single field slow-roll inflation yields a primordial non-Gaussian component roughly 100 times smaller than that induced by gravitational mode-couplings [2, 3]. The two terms are additive, so recovering this latter primordial signal is next to impossible, even before contending with cosmic variance. Multi-field models may generate larger non-Gaussianities [4, 5, 6, 7, 8], but this is by no means a generic property of these scenarios. Consequently, the detection of a primordial 3-point function would immediately falsify a very large class of inflationary models. Conversely, non-slow-roll models with higher order derivative terms, such as DBI inflation [9, 10, 11, 12] and k-inflation [13, 14], do typically generate large non-Gaussianities [15]. Further references, include more complicated multi-field, non-local or ghost theories, can be found in Refs. [16, 17, 18, 19, 20, 21, 22, 23, 24]. In this paper we investigate simple models – in the sense that they are driven by a single, minimally coupled scalar field with a canonical kinetic term – which generate substantial non-Gaussianities.

Constraining the non-Gaussian signal in a CMB dataset is a highly non-trivial problem. Firstly, it depends on the choice of estimators. At the moment, only two concrete estimators have been constructed: the f_{NL}^{local} and f_{NL}^{equil} forms [25, 26, 27, 28, 29, 30, 31], and both are

scale-invariant. The recent claim of a detection of a non-zero 3-point function [32] in the WMAP 3-year data [28] relies on the estimator developed in Ref. [31, 29, 26] which is of the “local” form [33, 25]. However non-Gaussianities that have strong scale dependence are not well-described by f_{NL}^{local} and f_{NL}^{equil} , and will require scale-dependent estimators, based on theoretically motivated ansatzen for the primordial non-Gaussianities. In addition to computing the primordial 3-point term, comparing the predictions of a specific inflationary model to the CMB requires us to evolve this signal through to recombination, and to project it onto the sphere on the sky, which is a convolution of the primordial 3-point term with 3 l -valued spherical Bessel functions. In general, this process is computationally expensive but simplifies dramatically if the 3-point function has special algebraic properties [34, 35].

Using Maldacena’s elegant formalism [3], the primordial 3-point curvature correlation function is computed via a set of integrals (over time) of products of three mode functions (or their derivatives) and slow roll parameters. Looking at these integrals, we identify two mechanisms which can create substantial non-Gaussianities. The first class consists of potentials with a localized violation of slow roll. This can take the form of a small localized feature, including the step models [36, 37] whose 3-point term was first accurately computed by the present authors in [38]. In addition models with a short inflationary phase can have initial transients in their dynamics, which will not be fully erased before the longest modes leave the horizon. In these cases, the 3-point term for modes which are leaving the horizon during the violation of slow roll can be magnified by three orders of magnitude, without ruining the fit to the 2-point function. The second class arises when a small ripple is superimposed on top of an otherwise smooth potential. This induces a “resonance” inside one of these integrals, giving the 3-point function a substantial amplitude *before* the modes cross the horizon. In the former case the 2-point function may be substantially modified; in the second case the modification of the 2-point function is very small, even though the 3-point function is large. The latter mechanism has not been described previously and the seemingly contrived field theoretic potential may in fact arise naturally in brane inflation models [39].

With this information in hand, we construct rough analytic approximations to the corresponding 3-point terms. These expressions have the factorizable form required by [34], which means that we can efficiently compute constraints on step potentials or similar models from CMB data, although at this point we are only interested in a qualitative match to the numerically computed 3-point term. We check our semi-analytic estimates for the 3-point function using an improved version of the code described in [38], which has a much cleaner scheme for removing numerical divergences in the 3-point integrals. The integrands are products of large, rapidly oscillating terms. Analytically, these are finite, but their *numerical* evaluation is non-trivial, and we show how to transform them into an explicitly finite form before the numerical evaluation is carried out. From a practical perspective, this means we can compute the 3-point function for “triangles” which contain two very different scales.

The paper is organized as follows. In Section 2 we review the computation of the 3-point function, and in Section 3 we describe the numerical algorithm. Sections 4 and 5 discuss the two distinct *mechanisms* for generating large primordial non-Gaussianities within minimally coupled single scalar field inflation, and we derive the approximate analytic ansatzen for the 3-point function. We then use our numerical methods to compute the exact 3-point function for these models, and show that these approximations yield fair representations of

the underlying non-Gaussianities. In Section 6 we summarize and discuss our results and plans for future work. We follow the notational conventions of [38] and set the reduced Planck mass M_p to unity except when presenting final results or defining parameter values.

2 Single scalar field inflation models and Maldacena's formalism

Consider scalar field inflation with an arbitrary potential

$$S = \int dx^4 \sqrt{g} \left[\frac{R}{2} - \frac{1}{2}(\partial\phi)^2 - V(\phi) \right]. \quad (2.1)$$

During inflation, spacetime is described by the Friedman-Robertson-Walker metric

$$ds^2 = -dt^2 + a^2(t)(dr^2 + r^2 d\Omega) = a^2(-d\tau^2 + dr^2 + r^2 d\Omega), \quad (2.2)$$

and the conformal time τ runs from $-\infty$ to 0. Dots denote derivatives by cosmic time t while primes denote derivatives with respect to τ .

The evolution of the single scalar field is described by

$$\phi'' + 2\frac{a'}{a}\phi' + \frac{1}{a^2}\frac{dV}{d\phi} = 0, \quad (2.3)$$

while the scale factor obeys the Friedmann equation

$$H = \frac{\dot{a}}{a} = \frac{1}{3} \left[\frac{1}{2}(\partial\phi)^2 + V(\phi) \right]. \quad (2.4)$$

The solution of the scalar field to these coupled set of equations is the trajectory of the scalar field in phase space $(\phi(t), \dot{\phi}(t))$. We can also describe this trajectory with the slow-roll parameters [40]

$$\epsilon = -\frac{1}{a} \frac{H'}{H^2}, \quad (2.5)$$

$$\eta = \frac{\dot{\epsilon}}{\epsilon H} = \frac{1}{a} \left[\frac{H''}{HH'} - a - 2\frac{H'}{H^2} \right]. \quad (2.6)$$

Slow-roll inflaton occurs when $|\epsilon| \ll 1$ and $|\eta| \ll 1$.

Since we are interested in models with complicated potentials, we will need to solve their perturbation equations numerically, before deriving analytical approximations to the 3-point functions. Moreover, we will need to track the perturbations while they are inside the horizon, and thus cannot resort to the large wavelength approximation [8, 41, 42, 43]. Instead we use the approach introduced by Maldacena [3], in what follows we use the notation of both this paper and Ref. [44].

We first split the Hamiltonian into its quadratic component H_0 and its higher order interaction component H_I ,

$$H[\delta\phi, \delta g_{\mu\nu}] = H_0[\delta\phi^I, \delta g_{\mu\nu}^I] + H_I[\delta\phi^I, \delta g_{\mu\nu}^I]. \quad (2.7)$$

The superscript I signifies that these modes are evolved using the linear (i.e. free field) equations of motion. Since we are interested only in the 3-point correlation functions, H_I contains terms up to third order in linear variables.

One can then show (see the Appendix of [44]) that any given combination of product of fields Q , can be evolved by a simple unitary transform

$$Q(t) = \left[\bar{T} \exp \left(i \int_{t_0}^t H_I(t) dt \right) \right] Q^I(t) \left[T \exp \left(-i \int_{t_0}^t H_I(t) dt \right) \right]. \quad (2.8)$$

Here \bar{T} and T refer to anti-time-ordering and time-ordering, but since we have only third order terms, the time ordering is not a factor in the equation. Using Eq. (2.8) [3], the 3-point correlation function for the Bardeen curvature ζ [45] is

$$\langle \zeta(\tau, \mathbf{k}_1) \zeta(\tau, \mathbf{k}_2) \zeta(\tau, \mathbf{k}_3) \rangle = -i \int_{\tau_0}^{\tau} d\tau' a \langle [\zeta(\tau, \mathbf{k}_1) \zeta(\tau, \mathbf{k}_2) \zeta(\tau, \mathbf{k}_3), H_I(\tau')] \rangle. \quad (2.9)$$

This is well-suited to numerical calculations, as we now simply need to solve for the Fourier mode of the linear order perturbation in order to compute the relevant integrals.

The main advantage of Maldacena's approach is the usage of the ADM formalism, where the constraint equations can be conveniently solved and interaction terms expanded. The computation of H_I for a minimally coupled single field inflationary model was performed in detail in Ref. [3]. It has the general form

$$H_I = \int dx^3 \sum_i a^2 g_i(\epsilon, \eta, \eta') \xi_1 \xi_2 \xi_3, \quad (2.10)$$

where ξ denotes either ζ , ζ' or $\partial\zeta$, and g_i are functions of the slow-roll parameters $\epsilon(t)$ and $\eta(t)$. We see that the coupling strength of the interaction Hamiltonian depends on the dynamics of the background encoded by the slow-roll parameters. We emphasize that this equation is *exact* to all orders in slow-roll parameters, and *does not depend on the slow-roll conditions*. In other words, even if we violate the slow roll conditions these equations still hold. In order to compute the 3-point function, we must evaluate the set of integrals listed in Appendix A. It is now clear why standard single field slow roll inflation does not generate large non-Gaussianities: the interaction couplings are functions of the slow-roll parameters, and hence are small by construction. However, large non-Gaussianities are possible if these couplings behave in a non-trivial way while keeping the viability of the power spectrum.

3 Numerical integration

Our goal is to integrate Eqs. (2.9) and (2.10) numerically. We first numerically solve the background and linear order equations of motion for the fields using the free field Hamiltonian – to do this we solve the relevant equations of motion using a standard Runge-Kutta 6th order integrator. We then plug the solution into Eq. (2.9) and integrate them from $-\infty < \tau < 0$ to obtain the 3-point function.

The integrals (see Appendix A for the explicit formulas) possess the generic form

$$I \propto \Re \left[\prod_i u_i(\tau_{end}) \int_{-\infty}^{\tau_{end}} d\tau a^2 g(\epsilon, \eta, \eta') \xi_1(\tau) \xi_2(\tau) \xi_3(\tau) \right] \quad (3.11)$$

where ξ can denote $\zeta(\vec{k})$ or $d\zeta(\vec{k})/d\tau$, and g is some function of the slow roll parameters which differs from term to term. These integrals are formally convergent in the limit $\tau \rightarrow -\infty$, but cutting them off at a finite value of τ exposes the oscillatory nature of the integrand whose amplitude blows up rapidly as τ grows large and negative, introducing a spurious contribution of $\mathcal{O}(1)$. Physically, when the modes are well within the horizon, they oscillate rapidly compared to the rate of change of the interaction terms, so the contribution to the integrals almost cancels. We can see this by rotating the integrals $\tau \rightarrow \tau(1 + i\epsilon)$ into the imaginary plane, giving the oscillatory part of the integral a damping term at large negative τ [3, 46, 15].

In [38], we added in a damping factor $e^{-\beta\tau}$ by hand to regulate the integrals, but this tends to systematically underestimate the resulting integrals, and β needs to be chosen carefully to balance accuracy and computational efficiency. However, we can regulate these integrals analytically, so that the numerical evaluation involves an explicitly finite integrand. We start by splitting the integral in Eq. (3.11) into two parts

$$I = \int_{-\infty}^{\tau_{end}} = \int_{-\infty}^{\tau_0} + \int_{\tau_0}^{\tau_{end}} = I_1 + I_2. \quad (3.12)$$

Here τ_0 is an arbitrary time when all three modes are well inside the horizon, and τ_{end} corresponds to a moment long after horizon exit. It is straightforward to numerically evaluate I_2 , but I_1 suffers from the cut-off dependence we mentioned earlier.

When all three modes are well inside the horizon, their phase and amplitude is well-described by the WKB approximation [47]¹.

$$v_k \approx \frac{1}{\sqrt{2\alpha(k)}} \exp \left[i \int \sqrt{\alpha(k)} d\tau \right] + \text{c.c.}, \quad (3.13)$$

where $\alpha(k) = k^2 + z''/z$. Deep within the horizon, $k^2 \gg z''/z$, the modes would not see the curvature term and hence it will propagate as a plane wave $v_k \propto \exp[ik\tau]/\sqrt{k}$. Specializing to the case $\xi = \zeta$ for now

$$I_1 = \int_{-\infty}^{\tau_0} d\tau \theta(\tau) \frac{1}{\sqrt{8k_1 k_2 k_3}} e^{iK(\tau-\tau_0)} \quad (3.14)$$

where $K \equiv k_1 + k_2 + k_3$ and we set

$$v(\tau_0) = \frac{1}{\sqrt{2k}}, \quad v'(\tau_0) = \frac{ik}{\sqrt{2k}}, \quad (3.15)$$

¹The 2-point function is computed with WKB methods in [48]. Here we only need the mode evolution inside the horizon, while a full treatment requires matching across the moment of horizon crossing, using standard turning point techniques.

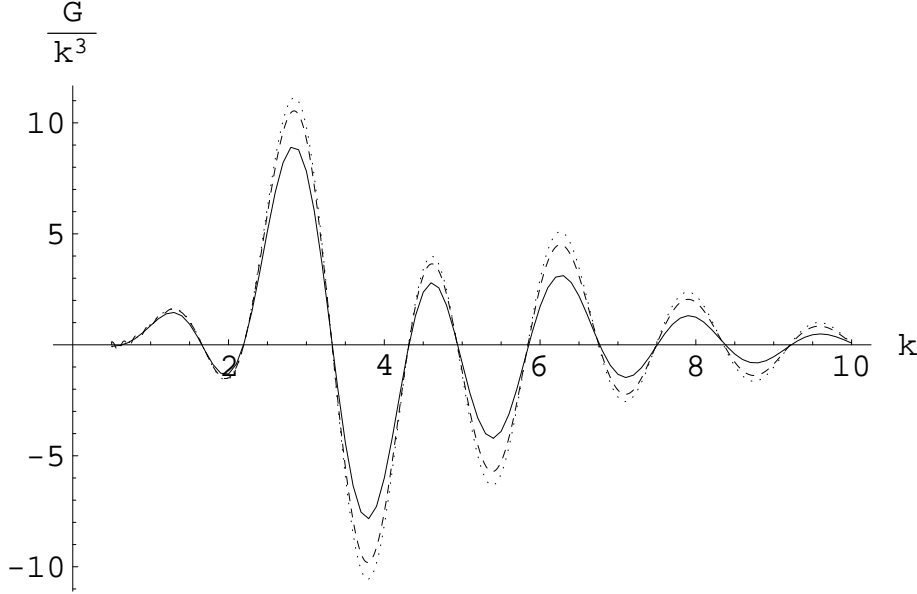


Figure 1: This plot compares the 3-point correlation function, computed using the β described in [38] and the boundary regulator described in this section, in the case of the step model [Sec. 4.1 with model parameters $(c, d, \phi_s) = (0.0018, 0.022M_p, 14.84M_p)$]. We plot the dimensionless variable G/k^3 defined in Eq. (4.20) for the equilateral case. The solid and the dashed lines are results obtained $\beta = 0.01$ and $\beta = 0.005$ respectively, while the dotted line is the result obtained from using the boundary regulator. The value of β is chosen such that it gives optimal results at around $k = 1$; if β is too small the early time oscillation will not be suppressed while if β is too large it will over-suppress the high k values. The boundary regulator does not suffer from this arbitrariness, and matches the limit found when $\beta \rightarrow 0$.

and θ is some function of τ given by

$$\theta(\tau) = \frac{a^2}{z^3} g(\epsilon, \eta, \eta'). \quad (3.16)$$

In general, θ diverges as $\tau \rightarrow -\infty$, but there is always some finite value of p such that $\theta(\tau)\tau^p \rightarrow 0$ as $\tau \rightarrow -\infty$.

Now integrate Eq. (3.14) by parts

$$I_1 = \frac{1}{\sqrt{8k_1k_2k_3}} \frac{-i}{K} \theta(\tau) e^{iK(\tau-\tau_0)} \Big|_{-\infty}^{\tau_0} - \int_{-\infty}^{\tau_0} d\tau \frac{d\theta}{d\tau} \frac{1}{\sqrt{8k_1k_2k_3}} \frac{-i}{K} e^{iK(\tau-\tau_0)}. \quad (3.17)$$

The boundary term at $-\infty$ is apparently divergent, but if we use the same ϵ rotated contour as before, so $-\tau \rightarrow -\infty(1+i\epsilon)$ the term vanishes for any finite value of ϵ . The remaining integral is now *more* convergent at large negative τ since the integrand has picked up a factor $\propto \tau^{-1}$. Integrating by parts a second time we find

$$I_1 = \frac{1}{\sqrt{8k_1k_2k_3}} \left[\frac{-i}{K} \theta(\tau_0) - \left(\frac{-i}{K} \right)^2 \frac{d\theta}{d\tau}(\tau_0) \right] + \int_{-\infty}^{\tau_0} d\tau \frac{d^2\theta}{d\tau^2} \frac{1}{\sqrt{8k_1k_2k_3}} \left(\frac{-i}{K} \right)^2 e^{iK(\tau-\tau_0)}. \quad (3.18)$$

The resulting integral is now convergent for any F we encounter in this work, and can be evaluated efficiently. We could repeat this process to further speed the convergence of the remaining integral, but in practice this is not necessary. We illustrate the effectiveness of this “boundary regulator” in Figure 1.

4 Horizon scale generation of non-Gaussianities

In this section, we explore models of inflation where the non-Gaussianities are generated when the modes cross the horizon. Typically these models require a violation of slow-roll at some fixed physical scale. All modes experience a temporary boost in their coupling strengths courtesy of this violation, but only modes exiting the horizon as the violation occurs receive a boost in their non-Gaussian signatures. Modes deep within the horizon are still rapidly oscillating, and the net contribution to their non-Gaussianities cancel. The violation of slow roll can have two origins. The first is a potential with a localized feature, as discussed in [38], and we now generalize this analysis. Secondly, if the duration of inflation is such that initial transients in the dynamics have not been erased before observable modes leave the horizon [49] we again find a significantly boosted 3-point function at these scales, even though the *potential* is smooth.

4.1 Features in the inflationary potential

Consider a small step in the inflaton potential [36]. In the limit that the step is a genuine discontinuity, the change in the potential energy across the step would be entirely converted into the inflaton’s kinetic energy, which is then damped away. For realistic models $\Delta V/V < 0.01$ so $\dot{\phi}^2/2 \ll V$ across the step, and $\epsilon \ll 1$. Recall that we are working in the Hubble slow roll formalism – if we had defined $\epsilon \propto (V_{,\phi}/V)^2$ this quantity can become large across the step. Further, η is the rate of change of ϵ , so η and η' can become large, provided they do so over a small enough range in ϕ . Features are thus associated with a characteristic physical scales and thus generate scale-dependent power spectra and higher correlation functions [38].

The 3-point correlation function $\langle \zeta(\mathbf{k}_1)\zeta(\mathbf{k}_2)\zeta(\mathbf{k}_3) \rangle$ is dominated by the $\epsilon\eta'$ term [38],

$$i \left(\prod_i u_i(\tau_{end}) \right) \int_{-\infty}^{\tau_{end}} d\tau a^2 \epsilon \eta' \left(u_1^*(\tau) u_2^*(\tau) \frac{d}{d\tau} u_3^*(\tau) + \text{sym} \right) (2\pi)^3 \delta^3 \left(\sum_i \mathbf{k}_i \right) + \text{c.c.} \dots \quad (4.19)$$

In [38], we introduced the \mathcal{G} to describe non-Gaussianities with both shape and scale dependence:

$$\frac{\mathcal{G}(k_1, k_2, k_3)}{k_1 k_2 k_3} \equiv \frac{1}{\delta^3(\mathbf{k}_1 + \mathbf{k}_2 + \mathbf{k}_3)} \frac{(k_1 k_2 k_3)^2}{\tilde{P}^2 (2\pi)^7} \langle \zeta(\mathbf{k}_1)\zeta(\mathbf{k}_2)\zeta(\mathbf{k}_3) \rangle, \quad (4.20)$$

where \tilde{P} is a constant, and for convenience we set it to be roughly equal to the magnitude of the power spectrum, $\tilde{P}^2 \equiv 4 \times 10^{-10}$. In the absence of the sharp feature, (4.20) reduces to the local form with $\mathcal{G} = (3/10) f_{NL}^{local} \sum k_i^3$ in WMAP’s convention. We now construct an analytic approximation to this function.

To illustrate our approach, we consider two specific features, the step [36, 38]

$$V(\phi) = \frac{1}{2} m^2 \phi^2 \left[1 + c \tanh \left(\frac{\phi - \phi_s}{d} \right) \right], \quad (4.21)$$

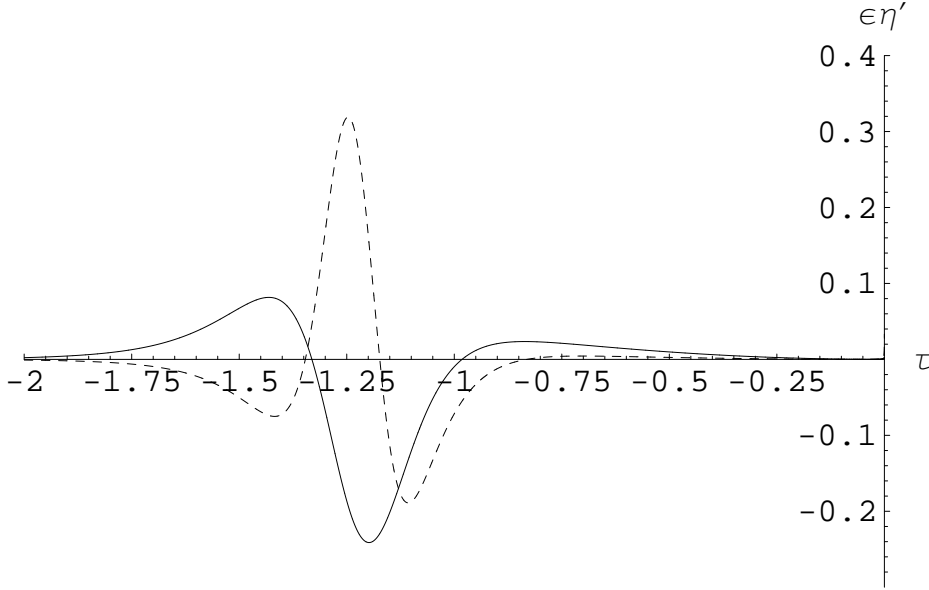


Figure 2: The evolution of $\epsilon \times \eta'$ with units $k_* \tau = -1.2$ where $k_* = 1$ is set to be the scale when ϕ crosses the center of the feature for our two models. The step ($c = 0.0018, d = 0.022M_p, \phi_s = 14.84M_p$) is the solid line, and bump is the dashed line ($c = 0.0005, d = 0.01M_p, \phi_b = 14.84M_p$). In both cases η' is boosted by $\mathcal{O}(1000)$ boost for around one Hubble time ($\delta\tau \approx 1$ in our units).

and the bump

$$V(\phi) = \frac{1}{2}m^2\phi^2 \left[1 + c \operatorname{sech} \left(\frac{\phi - \phi_b}{d} \right) \right], \quad (4.22)$$

where c , d and ϕ_b again respectively determines the height, width and location of the feature. In the latter case, c must be small enough to ensure that the field point does not get trapped in a local minimum. We present the numerical results for $\epsilon\eta'$ in Fig. 2 and the non-Gaussianity profile in Figure 3.

As we see from Fig. 2, η' is non-trivial over a small range of τ , but we do not have an analytic result for $u_i(\tau)$, and in [38] we performed these integrals numerically. Now consider a series of hat functions, $\eta' = \eta'_m \equiv \text{constant}$, for $\tau_m - \delta\tau_m < \tau < \tau_m + \delta\tau_m$, and 0 otherwise. Outside the range of these hat functions, $\eta = \mathcal{O}(\epsilon) \approx 0$, so

$$\int d\tau \eta' = 2 \sum_m \eta'_m \delta\tau_m \approx 0. \quad (4.23)$$

Namely, the area under the hat functions or the numerical curve of η' should sum to approximately zero. We approximate $\zeta(k_i)$ by its unperturbed form

$$\zeta(k_i) = \frac{iH}{\sqrt{4\epsilon k_i^3}} (1 + ik_i\tau) e^{-ik_i\tau}, \quad (4.24)$$

although the actual mode functions can deviate from this simple form by as much as a factor

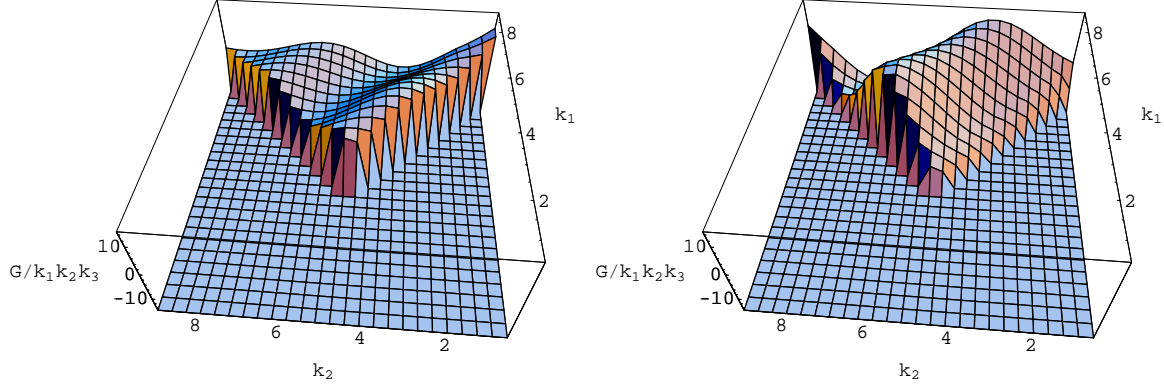


Figure 3: A sample result of the step (left) and bump (right) models, where for both plots $k_3 = 9$. We numerically computed the 3-point correlation functions of both models for $1 < k < 9$ such that $k = 1/1.2$ corresponds to the scale of the feature at $\phi_s = 14.84M_p$. For the step model, we use $(c = 0.0018, d = 0.022)$ while for the bump model we use $(c = 0.0005, d = 0.01)$.

of two (in addition to phase shifts) for short periods of time [36]. Using these approximations,

$$\begin{aligned}
\langle \zeta(\mathbf{k}_1)\zeta(\mathbf{k}_2)\zeta(\mathbf{k}_3) \rangle &\approx i \frac{H^4}{64\epsilon^3 \prod_i k_i^3} (2\pi)^3 \delta^3(\sum_i \mathbf{k}_i) \\
&\times \sum_m \epsilon \eta'_m \int_{\tau_m - \delta\tau_m}^{\tau_m + \delta\tau_m} \frac{d\tau}{\tau} (1 - i(k_1 + k_2)\tau - k_1 k_2 \tau^2) k_3^2 e^{iK\tau} \\
&+ \text{sym} + \text{c.c.} \tag{4.25}
\end{aligned}$$

$$\begin{aligned}
&= (2\pi)^7 \delta^3(\sum_i \mathbf{k}_i) P_k^2 \frac{1}{\prod_i k_i^3} \times \sum_m \frac{\eta'_m}{8} \left[- \sum_i k_i^2 \text{ImEi}(iK\tau) \right. \\
&\quad \left. + \frac{\sum_{i \neq j} k_i k_j^2}{K} \sin K\tau - \frac{k_1 k_2 k_3}{K} (\sin K\tau - K\tau \cos K\tau) \right]_{\tau_m - \delta\tau_m}^{\tau_m + \delta\tau_m}, \tag{4.26}
\end{aligned}$$

where

$$K \equiv k_1 + k_2 + k_3, \tag{4.27}$$

and $\text{ImEi}(iK\tau)$ denotes the imaginary part of the exponential integral function. For $K\tau \gg 1$, $\text{ImEi}(iK\tau) \rightarrow -\pi - \cos(iK\tau)/(K\tau) + \mathcal{O}((K\tau)^{-2})$; for $K\tau \ll 1$, $\text{ImEi}(iK\tau) \rightarrow K\tau + \mathcal{O}((K\tau)^2)$.

For large K , $K\tau_m \gg 1$, Eq. (4.26) is dominated by the last term,

$$\frac{\mathcal{G}}{k_1 k_2 k_3} \sim -\frac{1}{4} \sum_m \eta'_m \tau_m \sin K\tau_m \sin K\delta\tau_m. \tag{4.28}$$

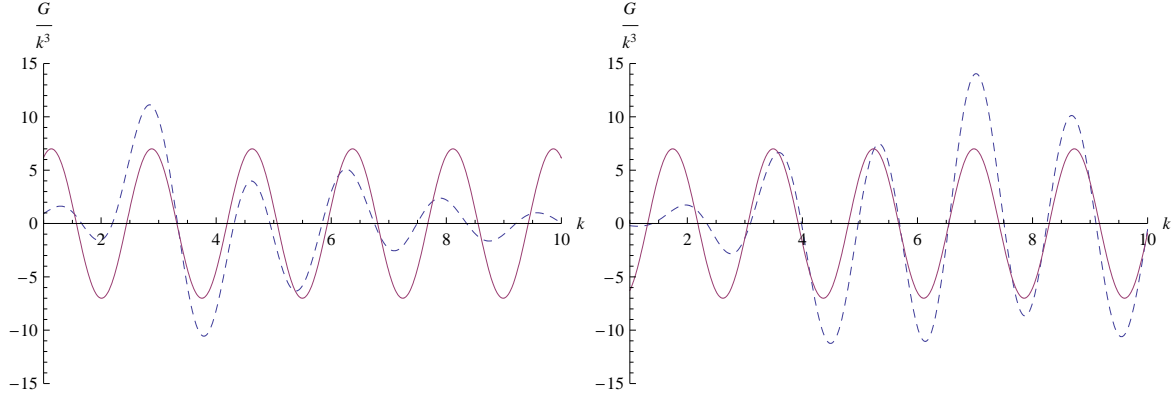


Figure 4: A comparison of the ansatz Eq. (4.31) (full line) to our numerical results (dashed line) for the step model ($c = 0.0018, d = 0.022$) on the left and the bump model ($c = 0.0005, d = 0.01$) on the right with $k_* \approx 1/1.2$. This is a reasonable match to our analytical from. As explained in the text, the drop-off at small and large k is not captured by the ansatz but can be easily incorporated by adding in a window function when comparing the ansatz with data. We have added a phase factor into the ansatz to synchronize with the numerical results; this phase factor is physically important but is not estimated analytically.

Numerically, the dominant scale-dependent oscillation comes from the term $\sin K\tau_m$, where τ_m is the center of the hat function, and corresponds to the moment the inflaton crosses the feature and $\phi(\tau_m) \approx \phi_s$. We denote this scale $-1/k_*$. The amplitude is further modulated by $\sin K\delta\tau_m$. Typically $\delta\tau_m \ll \tau_m$, so this term is less important unless the non-Gaussianities are found over a large k -range. From (4.23), we see the amplitude of (4.28) is roughly $\eta'\Delta\tau$ ($\Delta\tau$ is the duration of the feature in η'). This amplitude is consistent with the order-of-magnitude estimate of Ref. [38].

Before we write down the ansatz, let us take a step back and consider several other limits not well described by Eq. (4.28). For small K , $K\tau_m \ll 1$, and the leading terms (the first two terms in (4.26)) are proportional to $\sum_m \eta'_m \delta\tau_m \approx 0$. So the next order terms dominate,

$$\frac{\mathcal{G}}{k_1 k_2 k_3} \sim \sum_m \eta'_m \delta\tau_m \tau_m^2 K^2. \quad (4.29)$$

The non-Gaussianities vanish as $K\tau_m \rightarrow 0$ as these modes are outside the horizon as the inflaton encounters the feature.

In the squeezed triangle limit, $k_1 = k_2 = k$ and $k_3 \rightarrow 0$, the second term in (4.26) dominates instead of the third and we have a different behavior

$$\frac{\mathcal{G}}{k_1 k_2 k_3} \sim \sum_m \frac{\eta'_m}{4k_3} \cos 2k\tau_m \sin 2k\delta\tau_m. \quad (4.30)$$

Comparing (4.28) and (4.30), we see that the latter becomes more important if one of the momenta k_3 is smaller than $1/|\tau_m|$. This is less important observationally than Eq. (4.28), as it requires measurements on two widely different scales. In addition, Eq. (4.28) is incomplete also because it does not vanish for large K , and this is an artifact of the sharp edge of our

hat functions. We expect (4.28) to decay away after a width $\Delta K > 1/\delta\tau$ where $\delta\tau$ is the smoothing of the sharp edge of the hat function.

With these caveats in mind, we can now write down the ansatz following Eq. (4.28) by defining

$$\frac{\mathcal{G}_{\text{feat}}}{k_1 k_2 k_3} \equiv f_{\text{feat}} \sin\left(\frac{K}{k_*} + \text{phase}\right), \quad (4.31)$$

where we match the phase to our numerical results. We could improve this approach by taking a sum of a series of hat functions, so the final form of the 3-point correlation function would then be a sum over oscillatory functions

$$\frac{\mathcal{G}_{\text{feat}}}{k_1 k_2 k_3} = \sum_m f_{\text{feat}}^{(m)} \sin\left(\frac{K}{k_*^{(m)}} + \text{phase}\right), \quad (4.32)$$

where $k_*^{(m)}$ is the scale associated with the center of the m -th hat function, or further polish this result using an Euler-Maclaurin expansion. However, our primary goal here was to produce an analytic expression that mirrored the qualitative form of the 3-point function generated by a step, and in this we have succeeded. This expression is scale-dependent and thus differs from “local” and “equilateral” forms. Finally, this ansatz is clearly factorizable and in future work we will use it – in combination with the algorithms of [34] – to probe the ability of specific CMB experiments to recover this type of signal from data.

For the step potential [38],

$$f_{\text{feat}} \sim \frac{7c^{3/2}}{d\epsilon}, \quad (4.33)$$

where c and d are the height and width of the step respectively. This feature is approximately localized, with a single scale k_* . The derivation of the phase factor is not instructive and we obtained it by matching to our numerical results. Refs. [50, 51] use a step to explain the “glitch” seen in the temperature C_ℓ for $\ell \sim 30$, and find best fit parameters ($c = 0.0018$, $d = 0.022$, $\phi_s = 14.84M_p$). Looking at Fig. 4 we find

$$\frac{\mathcal{G}_{\text{feat}}}{k_1 k_2 k_3} = 7 \sin\left(\frac{K}{0.83} + \text{phase}\right). \quad (4.34)$$

The amplitude is within the order of magnitude that we expected from Eq. (4.33) and $\tau_m = -1/k_* \approx -1.2$ is indeed around the center of the feature in Fig. 2. These approximations are intended to capture the qualitative form of the 3-point function and do not have a high degree of numerical fidelity, but could certainly be further developed. Moreover, the detailed numerical match to the exact result could be improved substantially by adding heuristic parameters to the approximation, and then varying these to optimize the approximation.

4.2 Non-attractor initial conditions

Non-Gaussianities can also be enhanced if the inflaton trajectory is initially displaced from its attractor, slow-roll solution – for instance by giving it large kinetic energy (“fast-roll”) or perturbing the field point in a step direction, orthogonal to the inflaton trajectory. Hubble

friction will erase this transient, so this situation only arises when the overall duration of inflation is close to the minimal value. Again, modes that are crossing the horizon during this period have their non-Gaussianities boosted due to the enhanced coupling. In this case the relevant scales are the longest modes that contribute to the CMB.

This mechanism was used by Contaldi et. al. [49] to explain the possible low- l suppression in CMB (see also [52, 53]).² The inflaton is started with a large velocity and the potential is negligible, so

$$\ddot{\phi} + 3H\dot{\phi} \approx 0, \quad H^2 \approx \frac{\dot{\phi}^2}{6}. \quad (4.35)$$

One finds $a(t) \sim t^{1/3}$, and $\dot{\phi} \approx -\sqrt{6}/(3(t+t_0))$, where t_0 is determined by the initial velocity. During this fast-roll period,

$$\epsilon_f \approx 3, \quad \eta_f \approx 0. \quad (4.36)$$

In a qualitative estimate, Ref. [49] assumes that the slow-roll inflation period begins immediately after this kinetic-energy-dominated fast-roll (non-inflationary) period, and during slow-roll

$$\epsilon_s \approx \eta_s \approx 0.01. \quad (4.37)$$

Let us estimate the non-Gaussianity. For example, consider (A.69)

$$\frac{i}{2} \int_{\tau_{\text{begin}}}^{\tau_{\text{end}}} d\tau a^2 \epsilon^3 \left(\prod_i u_i(\tau_{\text{end}}) \right) \left(u_1^* \frac{du_2^*}{d\tau} \frac{du_3^*}{d\tau} \frac{\mathbf{k}_1 \cdot \mathbf{k}_2}{k_2^2} + \text{five perm} \right) (2\pi)^3 \delta^3 \left(\sum_i \mathbf{k}_i \right) + \text{c.c.} . \quad (4.38)$$

The fast-roll period is not inflationary, so modes are entering the horizon during this phase. As we will explain more quantitatively in Appendix B, we are interested in the modes that are slightly within the horizon as inflation begins. Modes that are near the horizon have smaller non-Gaussianities. Although the coupling $\epsilon_f \approx 3$ is greatly enhanced comparing to $\epsilon_s \approx 0.01$ in the slow-roll phase, the mode function $u_k \propto 1/\sqrt{\epsilon_f}$ is greatly suppressed. Looking at (4.38), we find the following factors of ϵ in the amplitude of the 3-point correlation

$$\frac{\mathcal{G}}{k^3} \sim f_{\text{fast}} \sim \epsilon_f^3 \epsilon_s^{-3/2} \epsilon_f^{-3/2} \epsilon_s^2. \quad (4.39)$$

The first factor is the large coupling; the second is due to the asymptotic value $u_k(\tau_{\text{end}})$, which is determined by the slow-roll inflation period; the third is from $u_k(\tau)$ during the fast-roll period – note this is where the suppression comes from; the fourth is from the prefactor, $1/\dot{P}^2 \propto \epsilon_s^2$, in the definition of \mathcal{G}/k^3 . This gives

$$f_{\text{fast}} \sim 0.5, \quad (4.40)$$

²Ref. [54] extended this approach to other non-inflationary initial conditions, and the same conclusion applies to this model. Conversely, [55] looks at a perturbation in a two-field model, which is beyond the scope of the current analysis.

which is confirmed by a more detailed estimate in Appendix B.

We next look at the transition period from the end of the fast-roll to the slow-roll, where ϵ drops from $\epsilon_f \approx 3$ to $\epsilon_s \approx 0.01$. This period is absent in the above analytical model of Ref. [49], but it also has important contribution to the non-Gaussianities. Once the kinetic and potential energies are roughly balanced, H is approximately constant, and $\dot{\phi}$ drops as e^{-3Ht} and ϵ drops as e^{-6Ht} . The η grows from 0 to $\mathcal{O}(1)$ at the beginning of this period, then drops to $\mathcal{O}(0.01)$ in the end. The most important contribution to the 3-point is the $\epsilon\dot{\eta}$ term, similarly to the sharp feature case, and possess the amplitude

$$f_{tran} = \mathcal{O}(\Delta\eta) = \mathcal{O}(1) . \quad (4.41)$$

The shape and running of this non-Gaussianity is also similar to those of the sharp feature, hence the ansatz (4.31) applies.

The sum of these two contributions implies that the 3-point is $\mathcal{O}(100)$ larger than the $f \approx \epsilon_s$ of standard slow-roll inflation. Our numerical simulation (not shown here) confirms this expectation. This is only comparable to the $f_{NL}^{local} = \mathcal{O}(1)$ 3-point expected from simple non-linear gravitational effects of [1], and an order of magnitude smaller than the 3-point we found for a bump. Since the kinetic energy is simply redshifted away by the expansion of the universe, we cannot easily enhance this signal by tuning the potential. Further, this signal peaks at scales where cosmic variance will be largest, so we are not optimistic this signal will be observable, even under ideal conditions.

5 Sub-horizon generation of non-Gaussianities: Resonance model

We now turn our attention to the generation of significant non-Gaussianities while the modes are still well within the horizon. Again, we inspect the integral representation of the 3-point correlation function, Eq. (3.11). Modes that are well within the horizon oscillate rapidly. Since the interaction couplings ϵ, η' are roughly constant for plain vanilla slow-roll model, these oscillations cancel. However, if the interaction couplings oscillate, they can interfere *constructively* with the rest of the integrand, yielding an enhanced 3-point signal. These contributions are generated while the modes are deep inside the horizon, and are thus physically distinct from the situation explored previously.

When all modes are inside the horizon, each of the 3-point integrals (3.11) consist of an oscillatory piece $\sim e^{i(k_1+k_2+k_3)\tau}$ and a prefactor $g(\epsilon, \eta')$ which is a function of the slow roll parameters. If the potential has a small oscillatory component, g becomes

$$g(\epsilon, \eta') \sim \alpha(1 + \delta \sin(\omega\tau)) , \quad (5.42)$$

where $\omega > H$, and $\delta \ll 1$. We assume that α, ω and δ change slowly over a single Hubble time, and treat them as constants in what follows. As the physical wavelength $a(t)/K$ increases, the mode will briefly resonate with the coupling term g when its frequency is roughly ω . During this resonance phase, the $\xi_1\xi_2\xi_3$ term in the integrand of (3.11) can interfere constructively $\sin(\omega\tau)$ and generate a large 3-point function. Conversely, destructive interference will generate no extra contribution to the 3-point function. See Fig. 5 for an illustration of the resonance effect.

amplitude

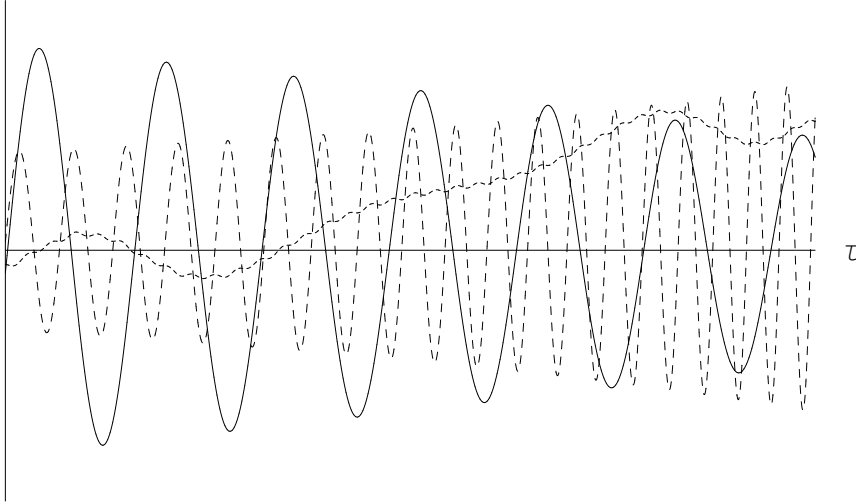


Figure 5: This figure illustrates resonance between the total mode $K = k_1 + k_2 + k_3$ momentum and an oscillatory η' . The solid line shows $\zeta(k)$, the dashed line describes η' , and the dotted line is the integral Eq. (3.11) from $-\infty$ to time τ with $k_1 = k_2 = k_3 = k$. Resonance occurs when the frequency of η' is roughly $3k$. This figure was generated after numerically evaluating the mode functions for the parameters of Eq. (5.46), with all the lines rescaled to arbitrary units to emphasise the effect. The universe grows by roughly one e-fold over the range of this plot, and the relevant modes are well inside the horizon.

This resonance requires

$$H < \omega < M_p , \quad (5.43)$$

in order to ensure that the relevant modes are sub-Planckian during the resonance epoch. In practice, this is not a strong constraint, but the resonance introduces a new length-scale into our analysis of cosmological perturbations.³ In this case, we expect non-Gaussianities to be present at all scales, since the ripple is laid down across the entire potential, in contrast to the “features” considered above. Moreover, the modulation of the potential must be small enough to ensure that the inflaton does not get trapped – and if we make it small enough, we can also ensure that the 2-point function is not significantly modified even if the non-Gaussianities are large, as discussed in Appendix C.

To study this mechanism explicitly, consider a standard slow-roll model with a very small oscillatory component

$$V(\phi) = \frac{1}{2}m^2\phi^2 \left[1 + c \sin \left(\frac{\phi}{\Lambda} \right) \right] . \quad (5.44)$$

Since ϕ is slowly rolling, the resonance effect occurs when the physical frequency reaches

$$\omega \approx \frac{\dot{\phi}}{2\pi\Lambda} = \frac{m}{\sqrt{6}\pi\Lambda} . \quad (5.45)$$

³In models with a non-trivial UV cutoff below the Planck scale, this scale would replace M_p in (5.43).

Therefore to satisfy the resonance condition (5.43), we need $\Lambda\phi \ll 1$ and $m \ll \Lambda$, while we take $H = m\phi/\sqrt{6}$, in accordance with slow roll. In Appendix C we show that we need $c\phi/\Lambda \ll 1$, so the perturbation to η is small.

Before we proceed, we emphasize that (5.44) is simply a toy model, with no direct physical motivation. However, in brane inflation, it has been argued that the duality cascade within a throat will leave tiny sharp features in the inflaton potential or the background warp factor [56]. Such features typically come in a series and can have cosmologically observable effects as the inflaton branes roll across them [39]. If these features are large and well-separated, they would yield of sequence of isolated sharp features. However, in the opposite limit, one would have a situation closer to the modulated potential above.

We now estimate the resulting 3-point function. For definiteness, we use the following parameters in our numerical examples

$$m = 3 \times 10^{-6} M_p \quad , \quad c = 5 \times 10^{-7} \quad , \quad \Lambda = 0.0007 M_p \quad , \quad \phi \approx 15 M_p \quad . \quad (5.46)$$

The non-Gaussianity oscillates with K because $g(\epsilon, \eta')$ has a continually changing phase. The time it takes the inflaton to cross one ‘‘ripple’’ is $\Delta t = \sqrt{6}\pi\Lambda/m$, during which $\Delta N_e = \pi\phi\Lambda$. So the oscillation period of this non-Gaussianity in K -space is

$$\Delta K = K\Delta N_e = \pi K\phi\Lambda \quad . \quad (5.47)$$

Using the parameters in (5.46), this gives $\Delta K/K = 0.033$. This agrees with the numerical results shown in Fig. 6. We emphasize that the property $\Delta K \propto K$ is model-independent, since, ignoring the slow-variation of background evolution, the analysis for Δt and ΔN_e is scale-independent. Another universal property is $\Delta K/K < 1$, via (5.43).

We now estimate the amplitude of these non-Gaussianities. The frequency of each mode is continuously decreasing due to the expansion of the universe. Once it differs from the resonant frequency by $\Delta\omega$, the integration in the 3pt starts to cancel out if it is performed over $\Delta t_1 \sim \pi/\Delta\omega$. Meanwhile, it takes $\Delta t_2 \sim \Delta\omega/(\omega H)$ to stretch a mode sufficiently in order to induce a frequency change ω to $\omega - \Delta\omega$. Equating Δt_1 and Δt_2 gives the time period over which resonance occurs for this particular mode,

$$\Delta t \sim \sqrt{\frac{\pi}{\omega H}} \quad . \quad (5.48)$$

In (5.44), this corresponds to the number of oscillation cycles

$$\frac{\Delta t}{T} \approx \frac{1}{\sqrt{\Lambda\phi}} \quad (5.49)$$

we need to integrate over, where $T = \sqrt{6}\pi\Lambda/m$ is the oscillation period of the background. For (5.46) we need about 10 cycles, which is confirmed numerically in Fig. 5.

The dominant source of 3-point terms – as for the ‘‘feature’’ models – is the $\epsilon\eta'$ interaction term Eq. (4.19). Because the mode is well within the horizon $|K\tau| \gg 1$, in (4.25) the last term dominates. Denoting the oscillatory behavior of the slow-roll parameter as

$$\dot{\eta} \supset \dot{\eta}_{\text{osci}} = \dot{\eta}_A \sin(\omega t) \quad , \quad (5.50)$$

where the subscript ‘‘A’’ denotes the oscillation amplitude. Integrating over one period

$$\int d\tau \tau \sin(\omega t) e^{iK\tau} \quad (5.51)$$

gives the amplitude $\pi\tau_*/K$, where $\tau_* = -1/aH$ is evaluated around the resonant point. Combining this with Eq. (5.49), from (4.25) we get the estimate of the amplitude

$$f_{\text{res}} \approx \frac{3}{8} \frac{\dot{\eta}_A}{H\sqrt{\Lambda\phi}}. \quad (5.52)$$

To evaluate (5.52), we need $\dot{\eta}$. For (5.44) the amplitude of the dominant oscillating term in $\dot{\eta}$ is (see Appendix C)

$$\dot{\eta}_A \approx \sqrt{6} \frac{cm\phi}{\Lambda^2}. \quad (5.53)$$

Note one might naively expect that $\dot{\eta} \sim V''' \sim c/\Lambda^3$, i.e. that it scales as Λ^{-3} . However this over predicts the amplitude by a factor of Λ^{-1} : although $\dot{\eta} \propto \ddot{H}$, since $\dot{H} = -\dot{\phi}^2/2$ via the scalar field equation of motion (2.3) and hence $\ddot{H} = -\dot{\phi}\ddot{\phi} = 3H\dot{\phi}^2 + V'\dot{\phi} \propto V'$. It follows that $\dot{\eta} \propto \ddot{H} \propto V''$. The crucial point is that one can always use Eq. (2.3) to eliminate one ϕ derivative of V in the derivation of \dot{H} ; in other words one cannot simply neglect the $\ddot{\phi}$ term in the equation of motion. Numerical computations of $\dot{\eta}$ show that this estimate Eq. (5.53) is accurate in both amplitude and scaling.

Combining (5.52) and (5.53), we get the amplitude

$$f_{\text{res}} \approx \frac{9}{4} \frac{cM_p^3}{\Lambda^{2.5}\phi^{0.5}}, \quad (5.54)$$

where we have restored M_p into the final answer. For (5.46), $f_{\text{res}} \sim 22$, which differs from matches to our exact numerical results shown in Fig. 6 by $\sim 30\%$. The numerical results also exhibit the $\mathcal{G}/k^3 \propto c/\Lambda^{2.5}$ scaling, as can be seen in Fig. 7.

The ansatz for the non-Gaussianity is therefore

$$\frac{\mathcal{G}}{k_1 k_2 k_3}_{\text{ansatz}} = f_{\text{res}} \sin(C \ln K + \text{phase}), \quad (5.55)$$

where

$$C = 2\pi K/\Delta K \approx 2/(\phi\Lambda). \quad (5.56)$$

The $\ln K$ comes from the fact [in Eq. (5.47)] that the oscillation period ΔK is proportional to K and the background ϕ dependence of $\Delta K/K$ is approximately scale-invariant. The value of C is determined by the oscillation frequency in the K -space. We also point out that the power spectrum has the same oscillatory frequency in K -space, due to the same reason that we stated before (5.47). See Fig. 8 in Appendix C for details. We compare this ansatz with the numerical result in Fig. 6. This ansatz is factorizable at least by Taylor-expanding $\ln K$ in a range smaller than K . Note unlike the ansatz for the feature (4.31) where the non-Gaussianities are peaked around some fixed scale k_* , the amplitude does not decay and is present at all scales. In addition, $K > \Delta K$ so it oscillates faster. As we noted above, the specific potential we consider is a toy model, but this analysis could be extended to more complicated modulations, or models where the modulation applied only over a finite range of field values.

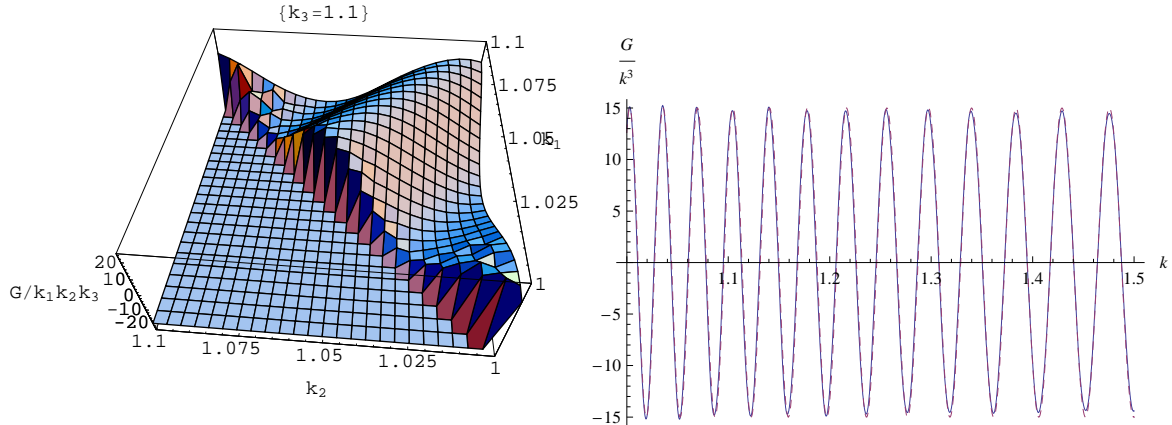


Figure 6: The numerical results for the 3-point correlation function of the resonance model. The plot on the left hand side is a 2-D slice of the 3-D function with fixed $k_3 = 1.1$ while k_2 and k_3 runs from 1.0 to 1.1. The plot on the right hand side is a comparison of the numerical result (full line) and our analytical ansatz (dashed line) for the equilateral case with $1.0 < k < 1.5$ – we have increased the range to more show the $1/K$ dependence of the frequency. The amplitude (5.54) over-predicts by about 30% – here we are have used instead numerically computed value of 15 to fit the plot better. On the other hand, the frequency (5.56) is accurate – we have used $C = 2.05/(\phi\Lambda)$ and added a phase factor to synchronize the plots.

6 Discussion and Conclusion

We studied two distinctly mechanisms for generating large non-Gaussianities within single field inflation. We derive the approximate 3-point correlation functions using semi-analytic methods, which are in the computationally useful *factorizable* form. In the first mechanism, non-Gaussianity is generated at horizon crossing by either a feature in the potential, or an initial transient in the inflationary dynamics. In the second case, oscillating slow roll parameters induce a resonance which leads to the generation of a non-Gaussian signal well before horizon crossing. In both cases, the 3-point function depends strongly on the individual wavelengths of the modes in the “triangle”. With a single, sharp feature or non-standard initial conditions, the 3-point is only enhanced in modes which are crossing the horizon as the inflaton traverses the “feature”. In a resonance model such as (5.44), the physical non-Gaussianity is present at all scales.

In the resonance case, we showed that the 3-point function is periodic with a period ΔK proportional to, and smaller than, $K = k_1 + k_2 + k_3$. This non-Gaussianity will peak starting from a fixed scale when projected onto the CMB sky. Assume for simplicity that $K \sim \ell$ where ℓ is the CMB multipole, and denote $\Delta\ell$ as the oscillation period. At larger scales where the oscillation spanning $\Delta\ell < 1$, this non-Gaussianity presumably cannot be resolved experimentally. For the numerical example considered here, it would become visible at $\ell \sim \mathcal{O}(100)$ where $\Delta\ell$ starts to exceed $\mathcal{O}(1)$, inducing an effective scale-dependence in this signal.

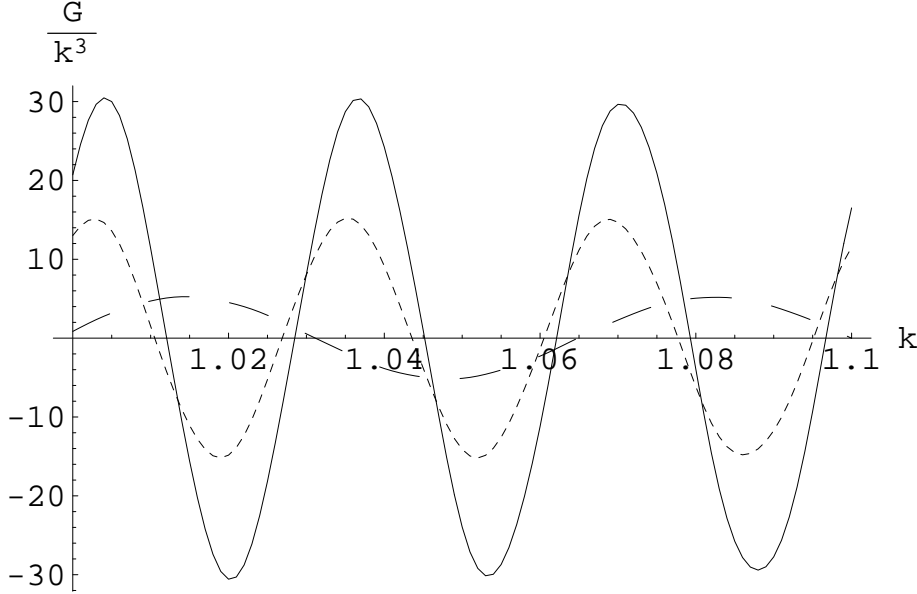


Figure 7: The numerical results for the set of parameters ($c = 5 \times 10^{-7}, \Lambda = 0.0007M_p$, shortdashed), ($c = 10 \times 10^{-7}, \Lambda = 0.0007M_p$, full) and ($c = 10 \times 10^{-7}, \Lambda = 0.0014M_p$, longdashed). The amplitude of the 3-point correlation function is proportional to $c/\Lambda^{2.5}$ while the frequency is independent of c and proportional to $1/\Lambda$.

With a feature in the potential, the resulting transient violation of slow-roll generically leads to an oscillatory and scale-dependent 3-point function. We wrote down a heuristic and factorizable scale-dependent expression for this signal and showed that it captured the qualitative properties seen in the exact numerical evaluations of the corresponding integrals. The 3-point correlation decays as we move away from $K \sim k_*$, where k_* corresponds to the scale leaving the horizon as the inflaton traverses the feature. We also show that while non-standard initial conditions such as the fast-roll model of [49] can generate large non-Gaussianities relative to our usual expectations for single field inflation, the amplification is not expected to lift them above the “noise” of non-linearities produced by post-inflationary gravitational evolution alone.

In addition, we have presented detailed description of a general numerical method for computing the 3-point correlation functions of primordial perturbations from canonical single scalar field inflationary models with arbitrary potentials. We show that while the integrals themselves are formally convergent, they need to be regularized as the integrands are oscillatory, and show how this can be accomplished analytically, rendering the numerical integrals rapidly convergent.

There is much further work to be done. Our immediate goal [57] is to use our heuristic ansatz to construct an optimal estimator with which to search for scale-dependent non-Gaussianities in the cosmic microwave background, and estimate the likely bounds that future missions can put on this signal. On the theoretical front, we plan to investigate the details of non-Gaussianities generated by multi-field models [5, 7] within the horizon, and with non-standard kinetic terms. Moreover, while the analytic approximations we present

here capture the qualitative form of the 3-point function, they are not intended to provide a precise quantitative match to the numerically computed values, but these approximations can certainly be improved.

Acknowledgments

We thank Eiichiro Komatsu, Henry Tye, Jiajun Xu, Hiranya Peiris, Kendrick Smith and Sarah Shandera for valuable discussions. XC and EAL would like to thank the Kavli Institute for Theoretical Physics in China and the organizers of the ‘‘String Theory and Cosmology’’ program, where part of this work is done, for their warm hospitality. XC is supported by the US Department of Energy under cooperative research agreement DEFG02-05ER41360. RE is supported in part by the United States Department of Energy, grant DE-FG02-92ER-40704.

A 3-point correlation functions

In minimally coupled single field inflation, the cubic interaction Hamiltonian for the scalar perturbation ζ is [3, 46, 15]

$$H_{int}(\tau) = - \int d^3x \left\{ a\epsilon^2 \zeta \zeta'^2 + a\epsilon^2 \zeta (\partial\zeta)^2 - 2\epsilon \zeta' (\partial\zeta) (\partial\chi) + \frac{a}{2} \epsilon \eta' \zeta^2 \zeta' + \frac{\epsilon}{2a} (\partial\zeta) (\partial\chi) (\partial^2\chi) + \frac{\epsilon}{4a} (\partial^2\zeta) (\partial\chi)^2 \right\}, \quad (\text{A.57})$$

where

$$\chi = a^2 \epsilon \partial^{-2} \dot{\zeta}. \quad (\text{A.58})$$

Here ∂^{-2} is the inverse Laplacian. This cubic Hamiltonian is exact for arbitrary ϵ and η .

The 3-point correlation function at some time τ after horizon exit is

$$\langle \zeta(\tau, \mathbf{k}_1) \zeta(\tau, \mathbf{k}_2) \zeta(\tau, \mathbf{k}_3) \rangle = -i \int_{\tau_0}^{\tau} d\tau' a \langle [\zeta(\tau, \mathbf{k}_1) \zeta(\tau, \mathbf{k}_2) \zeta(\tau, \mathbf{k}_3), H_{int}(\tau')] \rangle, \quad (\text{A.59})$$

together with a term coming from the field redefinition

$$\begin{aligned} \langle \zeta(\mathbf{k}_1) \zeta(\mathbf{k}_2) \zeta(\mathbf{k}_3) \rangle &= \langle \zeta_n(\mathbf{k}_1) \zeta_n(\mathbf{k}_2) \zeta_n(\mathbf{k}_3) \rangle \\ &+ \eta \langle \zeta_n^2(\mathbf{k}_1) \zeta_n(\mathbf{k}_2) \zeta_n(\mathbf{k}_3) \rangle + \text{sym} + \mathcal{O}(\eta^2 (P_k^\zeta)^3), \end{aligned} \quad (\text{A.60})$$

where $\zeta_n^2(\mathbf{k})$ denotes the Fourier transform of $\zeta_n^2(\mathbf{x})$.

We evaluate it using the decomposition

$$\zeta(\tau, \mathbf{k}) = u(\tau, \mathbf{k}) a(\mathbf{k}) + u^*(\tau, -\mathbf{k}) a^\dagger(-\mathbf{k}), \quad (\text{A.61})$$

$$v_k \equiv z u_k, \quad z \equiv a \sqrt{2\epsilon}, \quad (\text{A.62})$$

where $v(\tau, \mathbf{k})$ is the solution of the linear equation of motion of the quadratic action,

$$v_k'' + k^2 v_k - \frac{z''}{z} v_k = 0 . \quad (\text{A.63})$$

Our choice of vacuum implies that the initial condition for the mode function is given by the Bunch-Davies vacuum

$$\begin{aligned} v_k(\tau_0) &= \sqrt{\frac{1}{2k}} \\ v_k'(\tau_0) &= -i\sqrt{\frac{k}{2}} \end{aligned} \quad (\text{A.64})$$

where we have neglected an irrelevant phase.

We get seven contributions. The terms proportional to ϵ^2 arise from the $a^3 \epsilon^2 \dot{\zeta}^2$ term

$$2i \int_{-\infty}^{\tau_{end}} d\tau a^2 \epsilon^2 \left(\prod_i u_i(\tau_{end}) \right) \left(u_1^* \frac{du_2^*}{d\tau} \frac{du_3^*}{d\tau} + \text{two perm} \right) (2\pi)^3 \delta^3(\sum_i \mathbf{k}_i) + \text{c.c.} , \quad (\text{A.65})$$

the $a\epsilon^2 \zeta(\partial\zeta)^2$ term

$$-2i \int_{-\infty}^{\tau_{end}} d\tau a^2 \epsilon^2 \left(\prod_i u_i(\tau_{end}) u_i^*(\tau) \right) (\mathbf{k}_1 \cdot \mathbf{k}_2 + \text{two perm}) (2\pi)^3 \delta^3(\sum_i \mathbf{k}_i) + \text{c.c.} , \quad (\text{A.66})$$

and the $-2a\epsilon\dot{\zeta}(\partial\zeta)(\partial\chi)$ term

$$-2i \int_{-\infty}^{\tau_{end}} d\tau a^2 \epsilon^2 \left(\prod_i u_i(\tau_{end}) \right) \left(u_1^* \frac{du_2^*}{d\tau} \frac{du_3^*}{d\tau} \frac{\mathbf{k}_1 \cdot \mathbf{k}_2}{k_2^2} + \text{five perm} \right) (2\pi)^3 \delta^3(\sum_i \mathbf{k}_i) + \text{c.c.} . \quad (\text{A.67})$$

The term proportional to $\epsilon\eta$ is

$$i \left(\prod_i u_i(\tau_{end}) \right) \int_{-\infty}^{\tau_{end}} d\tau a^2 \epsilon \eta' \left(u_1^*(\tau) u_2^*(\tau) \frac{d}{d\tau} u_3^*(\tau) + \text{two perm} \right) (2\pi)^3 \delta^3(\sum_i \mathbf{k}_i) + \text{c.c.} . \quad (\text{A.68})$$

The terms proportional to ϵ^3 include that from $\epsilon/2a\partial\zeta\partial\chi\partial^2\chi$ term

$$\frac{i}{2} \int_{-\infty}^{\tau_{end}} d\tau a^2 \epsilon^3 \left(\prod_i u_i(\tau_{end}) \right) \left(u_1^* \frac{du_2^*}{d\tau} \frac{du_3^*}{d\tau} \frac{\mathbf{k}_1 \cdot \mathbf{k}_2}{k_2^2} + \text{five perm} \right) (2\pi)^3 \delta^3(\sum_i \mathbf{k}_i) + \text{c.c.} , \quad (\text{A.69})$$

and that from $\frac{\epsilon}{4a}(\partial^2\zeta)(\partial\chi)^2$ term

$$\frac{i}{2} \int_{-\infty}^{\tau_{end}} d\tau a^2 \epsilon^3 \left(\prod_i u_i(\tau_{end}) \right) \left(u_1^* \frac{du_2^*}{d\tau} \frac{du_3^*}{d\tau} k_1^2 \frac{\mathbf{k}_2 \cdot \mathbf{k}_3}{k_2^2 k_3^2} + \text{two perm} \right) (2\pi)^3 \delta^3(\sum_i \mathbf{k}_i) + \text{c.c.} . \quad (\text{A.70})$$

The field redefinition (A.60) contributes

$$\frac{\eta}{2} |u_2|^2 |u_3|^2 \Big|_{\tau \rightarrow \tau_{end}} (2\pi)^3 \delta^3(\sum_i \mathbf{k}_i) + \text{two perm} . \quad (\text{A.71})$$

In these equations, the “two perm” stands for two other terms that are symmetric under permutations of the indices 1, 2 and 3.

In Ref. [3, 46, 15] where sharp features and non-attractor initial condition are absent, terms (A.65), (A.66), (A.67) and (A.71) give the leading contributions to non-Gaussianities. In Ref. [38] where features are present on an otherwise flat potential, term (A.68) is the leading term. For the non-attractor initial condition that we consider in Sec. 4.2, the terms (A.69) and (A.70) can also give important contributions in addition to other terms, because ϵ and η can be large initially.

B Non-Gaussianities from initial conditions

In this appendix, we give some details on the estimate of non-Gaussianity from the fast-roll period discussed in Sec. 4.2. In terms of the conformal time τ , the scale factor of the fast-roll period becomes

$$a = \frac{h_s}{H_s} \sqrt{1 + 2h_s \tau} , \quad \tau_i \leq \tau \leq 0 . \quad (\text{B.72})$$

Here the fast-roll starts at $\tau = \tau_i$ and end at $\tau = 0$. h_s is the conformal Hubble parameter $h \equiv a'/a$ evaluated at the beginning the slow-roll inflation period (i.e. the end of the fast-roll period) $\tau = 0$. H_s is the corresponding Hubble parameter in terms of t , $H = h/a$. This fast-roll period is immediately connected to the inflation period in which the scale factor grows as

$$a = \frac{h_s/H_s}{1 - h_s \tau} , \quad 0 \leq \tau < 1/h_s . \quad (\text{B.73})$$

We first look at the power spectrum discussed in [49]. Using (B.72), one gets

$$2a^2 H^2 = \frac{2h_s^2}{(1 + 2h_s \tau)^2} , \quad (\text{B.74})$$

$$\epsilon \approx 3 , \quad \eta \approx 0 . \quad (\text{B.75})$$

From the definition $z \equiv a\sqrt{2\epsilon}$, we get

$$\frac{z''}{z} \approx -\frac{h_s^2}{(1 + 2h_s \tau)^2} . \quad (\text{B.76})$$

Picking a special initial condition for v_k , the equation of motion $v_k'' + k^2 v_k - \frac{z''}{z} v_k = 0$ can be solved as

$$v_k(\tau) = \sqrt{\frac{\pi}{8}} \frac{1}{\sqrt{h_s}} (1 + 2h_s \tau)^{1/2} H_0^{(2)}(k\tau + \frac{k}{2h_s}) , \quad (\text{B.77})$$

where $H_0^{(2)}$ is the second Hankel function with index 0. Requiring this solution and its first derivative to continuously match to the slow-roll results

$$v_k(\tau) = C_1 e^{-ik\tau + ik/h_s} \left(1 + \frac{i}{-k\tau + k/h_s} \right) + C_2 e^{ik\tau - ik/h_s} \left(1 + \frac{i}{k\tau - k/h_s} \right) \quad (\text{B.78})$$

at $\tau = 0$ determines the coefficients C_1 and C_2

$$\begin{aligned} C_1 &= \sqrt{\frac{\pi}{32h_s}} e^{-ik/h_s} \left[H_0^{(2)} \left(\frac{k}{2h_s} \right) - \left(\frac{h_s}{k} + i \right) H_1^{(1)} \left(\frac{k}{2h_s} \right) \right], \\ C_2 &= \sqrt{\frac{\pi}{32h_s}} e^{ik/h_s} \left[H_0^{(2)} \left(\frac{k}{2h_s} \right) - \left(\frac{h_s}{k} - i \right) H_1^{(1)} \left(\frac{k}{2h_s} \right) \right]. \end{aligned} \quad (\text{B.79})$$

The power spectrum is

$$P_k = \frac{H^2 k}{(2\pi)^2 \epsilon} |C_1 - C_2|^2. \quad (\text{B.80})$$

At large scale for $k \ll 2h_s$,

$$P_k \rightarrow \frac{H^2 k^3}{(2\pi)^3 \epsilon h_s^3} \left| \ln \frac{k}{2h_s} \right|^2. \quad (\text{B.81})$$

Hence we see that $P_k \rightarrow 0$ as $k \rightarrow 0$ resulting a suppression for the large scales. For $k \gtrsim h_s$, it relaxes to the usual attractor value $P_k = H^2/(8\pi^2 \epsilon)$.

Now we estimate the order of magnitude of the contribution to 3-point function by this fast-roll period. As an example, we look at the ϵ^3 terms (A.69) and (A.70). The ϵ^2 terms are expected to be of a similar size. We look at the modes $k \gtrsim h_s$ so the asymptotic value of u_k at the end of inflation τ_{end} is approximately that of the slow-roll inflation,

$$u_k(\tau_{end}) \approx \frac{iH_s}{\sqrt{4\epsilon_s k^3}} e^{-ik\tau}, \quad (\text{B.82})$$

as we see from the discussions in the last paragraph.

The net contribution of (A.69) and (A.70) to the 3pt is

$$- \frac{7\pi^{9/2}}{64} \frac{H_s^4}{k^{9/2} h_s^{3/2}} \left(\frac{\epsilon_f}{\epsilon_s} \right)^{3/2} \mathcal{R} \delta^3(\mathbf{k}_1 + \mathbf{k}_2 + \mathbf{k}_3), \quad (\text{B.83})$$

where

$$\mathcal{R} = \text{Re} \left[\int_{\frac{k}{2h_s} \left(\frac{H_s}{H_f} \right)^{2/3}}^{\frac{k}{2h_s}} dx x H_0^{(2)*}(x) H_1^{(2)*}(x) H_1^{(2)*}(x) \right]. \quad (\text{B.84})$$

We have integrated from the start of the fast-roll period τ_i to the beginning of the slow-roll period $\tau = 0$. We have written the lower limit of the integration in terms of the Hubble parameter at the beginning of the fast-roll, H_f .

Comparing to the WMAP's ansatz in the limit $k_1 = k_2 = k_3$

$$(2\pi)^7 \frac{9}{10k^6} f_{fast} P_k^2 \delta^3(\mathbf{k}_1 + \mathbf{k}_2 + \mathbf{k}_3) , \quad (\text{B.85})$$

we get a scale dependent amplitude for this fast-roll period

$$f_{fast} \approx -0.34 \left(\frac{k}{h_s} \right)^{3/2} \epsilon_s^{1/2} \epsilon_f^{3/2} \mathcal{R} . \quad (\text{B.86})$$

The integrand in (B.84) starts oscillating for large x . So for very large k , $k \gg 2h_s (H_s/H_f)^{2/3}$, this integration approaches zero. Therefore, we look at the modes $k \lesssim 2h_s (H_s/H_f)^{2/3}$. For example, for $k/h_s \approx 10$, $\epsilon_f \approx 3$, $\epsilon_s \approx 0.01$, $H_s/H_f \approx 0.1$, we have $\mathcal{R} = \mathcal{O}(1)$ and $f_{fast} \approx \mathcal{O}(0.2)$. This is consistent with the rough argument given in (4.39).

C Slow-roll parameters in the resonance model

In this appendix, we work out some details on the behavior of the slow-roll parameters in the resonant model. Using (5.44) as the explicit example, we decompose (and similarly for other variables)

$$\phi(t) = \phi_0(t) + \phi_{\text{osci}}(t) , \quad (\text{C.87})$$

where the ϕ_0 is the unperturbed background evolution, and ϕ_{osci} is the oscillation caused by the small high frequency ripples imposed on the potential. Since the oscillation frequency $\omega \gg H$, the equation of motion for the oscillatory part is

$$\ddot{\phi}_{\text{osci}} + (V')_{\text{osci}} \approx 0 , \quad (\text{C.88})$$

where the term $3H\dot{\phi}_{\text{osci}}$ is much smaller than $\ddot{\phi}_{\text{osci}}$ and neglected. The dominant contribution to $(V')_{\text{osci}}$ comes from

$$V_{\text{osci}} = \frac{1}{2} m^2 \phi^2 c \sin \frac{\phi}{\Lambda} . \quad (\text{C.89})$$

Using the background evolution

$$\phi_0(t) = -\frac{\sqrt{6}}{3} m t + \phi_i , \quad (\text{C.90})$$

we can solve (C.88) and get

$$\phi_{\text{osci}} \approx \frac{3}{4} c \phi_0^2 \Lambda \cos\left(\frac{\phi_0(t)}{\Lambda}\right) . \quad (\text{C.91})$$

With this result, one can check that (C.89) is indeed the leading oscillatory term in (5.44).

We next calculate the oscillatory part of H and \dot{H} . Differentiating

$$3H^2 = V + \dot{\phi}^2/2 , \quad (\text{C.92})$$

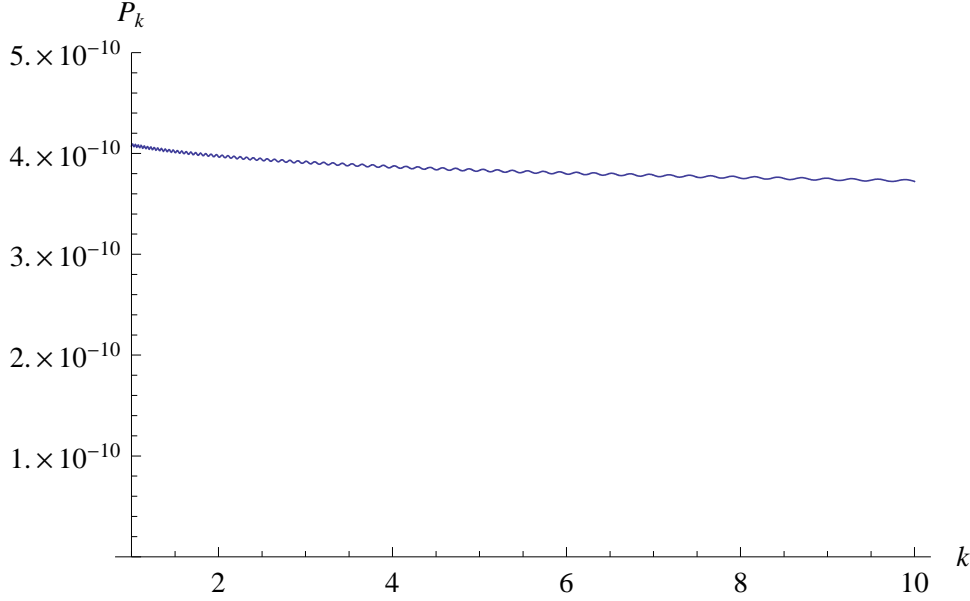


Figure 8: The power spectrum P_k for the resonance model. There is a small $\mathcal{O}(10^{-3})$ oscillation. The frequency (in k -space) is identical to that of the 3-point correlation function (in K -space) in Eq. (5.55). This is also different from the sharp feature case where the frequency (in k -space) of the power spectrum is twice of the frequency (in K -space) of the 3-point correlation function [38].

we get

$$\dot{H} = -\frac{1}{2}\dot{\phi}^2. \quad (\text{C.93})$$

So, we have

$$\frac{\dot{H}_{\text{osci}}}{\dot{H}_0} = -\frac{3c\phi_0^2}{2} \sin\left(\frac{\phi_0(t)}{\Lambda}\right). \quad (\text{C.94})$$

From (C.94), we get

$$\frac{H_{\text{osci}}}{H_0} = \frac{3c\phi_0\Lambda}{2M_p^2} \cos\left(\frac{\phi_0(t)}{\Lambda}\right). \quad (\text{C.95})$$

Note that if we try to get H_{osci} from (C.92), the leading terms will cancel and the subleading terms are not reliable in our approximation.

Now we calculate the oscillatory part of the slow-roll parameters. It is easy to see from the above results that the leading correction term for $\epsilon = -\dot{H}/H^2$ comes from that for \dot{H} , so

$$\begin{aligned} \epsilon_{\text{osci}} &\approx \epsilon_0 \frac{\dot{H}_{\text{osci}}}{\dot{H}_0} \\ &\approx -3c \sin\left(\frac{\phi_0(t)}{\Lambda}\right). \end{aligned} \quad (\text{C.96})$$

The leading correction term for $\eta = \dot{\epsilon}/(\epsilon H)$ comes from that for $\dot{\epsilon}$,

$$\begin{aligned}\eta_{\text{osci}} &\approx \eta_0 \frac{\dot{\epsilon}_{\text{osci}}}{\dot{\epsilon}_0} \\ &\approx \frac{3c\phi_0}{\Lambda} \cos\left(\frac{\phi_0(t)}{\Lambda}\right).\end{aligned}\tag{C.97}$$

Taking the time derivative of the above equation (C.97) we get

$$\dot{\eta}_{\text{osci}} \approx \sqrt{6} \frac{cm\phi}{\Lambda^2} \sin\left(\frac{\phi_0(t)}{\Lambda}\right),\tag{C.98}$$

which we can also derive directly by plugging in the potential Eq. (5.44) into the definition for η , Eq. (2.6), and keeping the leading oscillatory term.

The most important term in the linear equation of motion (A.63) is

$$\frac{z''}{z} = 2a^2 H^2 \left(1 - \frac{\epsilon}{2} + \frac{3}{4}\eta - \frac{1}{4}\epsilon\eta + \frac{1}{8}\eta^2 + \frac{1}{4}\frac{\dot{\eta}}{H}\right).\tag{C.99}$$

The most significant oscillating component comes from the last term

$$\frac{\dot{\eta}_{\text{osci}}}{4H} = \frac{3c}{2\Lambda^2} \sin\left(\frac{\phi_0(t)}{\Lambda}\right).\tag{C.100}$$

This term causes a dramatic oscillation of the freeze-out scale of the perturbation, which we define to be $a\sqrt{z/z''}$. For example, in terms of the numerical number (5.46), the amplitude of (C.100) is 1.53, of the same order of the non-oscillating component 1. The horizon size that we used in the main text refers to the averaged non-oscillating component. This oscillation affects the power spectrum, which we present numerically in Fig. 8. The oscillation in the power spectrum is tiny, but is potentially observable if the fidelity of our CMB data is very high. The structure of these oscillations is reminiscent of those of the ‘‘trans-Planckian’’ models of inflation, but with the distinctive scale-dependent oscillation frequency which has the same properties as we discussed at the end of Sec. 5 for the non-Gaussianity. For relevant details on constraining such oscillatory power spectrum on the CMB sky, see Ref. [58, 59].

References

- [1] T. Pyne and S. M. Carroll, Phys. Rev. D **53**, 2920 (1996) [arXiv:astro-ph/9510041].
- [2] V. Acquaviva, N. Bartolo, S. Matarrese and A. Riotto, Nucl. Phys. B **667**, 119 (2003) [arXiv:astro-ph/0209156].
- [3] J. M. Maldacena, JHEP **0305**, 013 (2003) [arXiv:astro-ph/0210603].
- [4] G. I. Rigopoulos, E. P. S. Shellard and B. J. W. van Tent, arXiv:astro-ph/0511041.
- [5] D. Seery and J. E. Lidsey, JCAP **0509**, 011 (2005) [arXiv:astro-ph/0506056].
- [6] F. Vernizzi and D. Wands, JCAP **0605**, 019 (2006) [arXiv:astro-ph/0603799].

- [7] T. Battefeld and R. Easther, *JCAP* **0703**, 020 (2007) [arXiv:astro-ph/0610296].
- [8] S. Yokoyama, T. Suyama and T. Tanaka, arXiv:0705.3178 [astro-ph].
- [9] E. Silverstein and D. Tong, *Phys. Rev. D* **70**, 103505 (2004) [arXiv:hep-th/0310221].
- [10] M. Alishahiha, E. Silverstein and D. Tong, *Phys. Rev. D* **70**, 123505 (2004) [arXiv:hep-th/0404084].
- [11] X. Chen, *Phys. Rev. D* **71**, 063506 (2005) [arXiv:hep-th/0408084].
- [12] X. Chen, *JHEP* **0508**, 045 (2005) [arXiv:hep-th/0501184].
- [13] C. Armendariz-Picon, T. Damour and V. F. Mukhanov, *Phys. Lett. B* **458**, 209 (1999) [arXiv:hep-th/9904075].
- [14] J. Garriga and V. F. Mukhanov, *Phys. Lett. B* **458**, 219 (1999) [arXiv:hep-th/9904176].
- [15] X. Chen, M. x. Huang, S. Kachru and G. Shiu, *JCAP* **0701**, 002 (2007) [arXiv:hep-th/0605045].
- [16] M. Li, T. Wang and Y. Wang, arXiv:0801.0040 [astro-ph].
- [17] R. Bean, D. J. H. Chung and G. Geshnizjani, arXiv:0801.0742 [astro-ph].
- [18] D. H. Lyth, C. Ungarelli and D. Wands, *Phys. Rev. D* **67**, 023503 (2003) [arXiv:astro-ph/0208055].
- [19] B. Chen, Y. Wang and W. Xue, arXiv:0712.2345 [hep-th].
- [20] S. Gupta, A. Berera, A. F. Heavens and S. Matarrese, *Phys. Rev. D* **66**, 043510 (2002) [arXiv:astro-ph/0205152].
- [21] I. G. Moss and C. Xiong, *JCAP* **0704**, 007 (2007) [arXiv:astro-ph/0701302].
- [22] N. Barnaby and J. M. Cline, arXiv:0704.3426 [hep-th].
- [23] N. Arkani-Hamed, P. Creminelli, S. Mukohyama and M. Zaldarriaga, *JCAP* **0404**, 001 (2004) [arXiv:hep-th/0312100].
- [24] C. Cheung, P. Creminelli, A. L. Fitzpatrick, J. Kaplan and L. Senatore, arXiv:0709.0293 [hep-th].
- [25] E. Komatsu and D. N. Spergel, *Phys. Rev. D* **63**, 063002 (2001) [arXiv:astro-ph/0005036].
- [26] E. Komatsu, D. N. Spergel and B. D. Wandelt, *Astrophys. J.* **634**, 14 (2005) [arXiv:astro-ph/0305189].
- [27] D. Babich, P. Creminelli and M. Zaldarriaga, *JCAP* **0408**, 009 (2004) [arXiv:astro-ph/0405356].

- [28] D. N. Spergel *et al.* [WMAP Collaboration], arXiv:astro-ph/0603449.
- [29] P. Creminelli, L. Senatore and M. Zaldarriaga, JCAP **0703**, 019 (2007) [arXiv:astro-ph/0606001].
- [30] P. Creminelli, L. Senatore, M. Zaldarriaga and M. Tegmark, JCAP **0703**, 005 (2007) [arXiv:astro-ph/0610600].
- [31] A. P. S. Yadav, E. Komatsu, B. D. Wandelt, M. Liguori, F. K. Hansen and S. Matarrese, arXiv:0711.4933 [astro-ph].
- [32] A. P. S. Yadav and B. D. Wandelt, arXiv:0712.1148 [astro-ph].
- [33] D. S. Salopek and J. R. Bond, Phys. Rev. D **42**, 3936 (1990).
- [34] K. M. Smith and M. Zaldarriaga, arXiv:astro-ph/0612571.
- [35] J. R. Fergusson and E. P. S. Shellard, arXiv:astro-ph/0612713.
- [36] J. A. Adams, B. Cresswell and R. Easther, Phys. Rev. D **64**, 123514 (2001) [arXiv:astro-ph/0102236].
- [37] E. Komatsu *et al.* [WMAP Collaboration], Astrophys. J. Suppl. **148**, 119 (2003) [arXiv:astro-ph/0302223].
- [38] X. Chen, R. Easther and E. A. Lim, JCAP **0706**, 023 (2007) [arXiv:astro-ph/0611645].
- [39] R. Bean, X. Chen, G. Hailu, S. H. Tye and J. Xu, arXiv:0802.0491 [hep-th].
- [40] D. S. Salopek and J. R. Bond, Phys. Rev. D **43** (1991) 1005.
- [41] M. Sasaki and E. D. Stewart, Prog. Theor. Phys. **95**, 71 (1996) [arXiv:astro-ph/9507001].
- [42] C. T. Byrnes, K. Koyama, M. Sasaki and D. Wands, arXiv:0705.4096 [hep-th].
- [43] D. H. Lyth and Y. Rodriguez, Phys. Rev. Lett. **95**, 121302 (2005) [arXiv:astro-ph/0504045].
- [44] S. Weinberg, Phys. Rev. D **72**, 043514 (2005) [arXiv:hep-th/0506236].
- [45] J. M. Bardeen, Phys. Rev. D **22** (1980) 1882.
- [46] D. Seery and J. E. Lidsey, JCAP **0506**, 003 (2005) [arXiv:astro-ph/0503692].
- [47] C. M. Bender and S. A. Orszag, *Advanced Mathematical Methods for Scientists and Engineers*, Springer-Verlag (1999).
- [48] J. Martin and D. J. Schwarz, Phys. Rev. D **67**, 083512 (2003) [arXiv:astro-ph/0210090].

- [49] C. R. Contaldi, M. Peloso, L. Kofman and A. Linde, JCAP **0307**, 002 (2003) [arXiv:astro-ph/0303636].
- [50] H. V. Peiris *et al.* [WMAP Collaboration], Astrophys. J. Suppl. **148**, 213 (2003) [arXiv:astro-ph/0302225].
- [51] L. Covi, J. Hamann, A. Melchiorri, A. Slosar and I. Sorbera, Phys. Rev. D **74**, 083509 (2006) [arXiv:astro-ph/0606452].
- [52] D. Boyanovsky, H. J. de Vega and N. G. Sanchez, Phys. Rev. D **74**, 123006 (2006) [arXiv:astro-ph/0607508].
- [53] D. Boyanovsky, H. J. de Vega and N. G. Sanchez, Phys. Rev. D **74**, 123007 (2006) [arXiv:astro-ph/0607487].
- [54] B. A. Powell and W. H. Kinney, Phys. Rev. D **76**, 063512 (2007) [arXiv:astro-ph/0612006].
- [55] C. P. Burgess, J. M. Cline, F. Lemieux and R. Holman, JHEP **0302**, 048 (2003) [arXiv:hep-th/0210233].
- [56] G. Hailu and S. H. Tye, JHEP **0708**, 009 (2007) [arXiv:hep-th/0611353].
- [57] X. Chen, R. Easther, E. Komatsu, H. Peiris, E. A. Lim and K. Smith, *In preparation*
- [58] T. Okamoto and E. A. Lim, Phys. Rev. D **69**, 083519 (2004) [arXiv:astro-ph/0312284].
- [59] R. Easther, W. H. Kinney and H. Peiris, JCAP **0508**, 001 (2005) [arXiv:astro-ph/0505426].